RANGER: A Monocular Zero-Shot Semantic Navigation Framework through Contextual Adaptation

Ming-Ming Yu[1,2], Yi Chen[3], Börje F. Karlsson[2†], Wenjun Wu[1,4,†]

[1]Beihang University, [2]Beijing Academy of Artificial Intelligence (BAAI),
[3]Institute of Automation, Chinese Academy of Sciences,
[4]Hangzhou International Innovation Institute, Beihang University

Abstract—Efficiently finding targets in complex environments is fundamental to real-world embodied applications. While recent advances in multimodal foundation models have enabled zero-shot object goal navigation, allowing robots to search for arbitrary objects without fine-tuning, existing methods face two key limitations: (1) heavy reliance on precise depth and pose information provided by simulators, which restricts applicability in real-world scenarios; and (2) lack of in-context learning (ICL) capability, making it difficult to quickly adapt to new environments, as in leveraging short videos. To address these challenges, we propose RANGER, a novel zero-shot, open-vocabulary semantic navigation framework that operates using only a monocular camera. Leveraging powerful 3D foundation models, RANGER eliminates the dependency on depth and pose while exhibiting strong ICL capability. By simply observing a short video of a new environment, the system can also significantly improve task efficiency without requiring architectural modifications or fine-tuning. The framework integrates several key components: keyframe-based 3D reconstruction, semantic point cloud generation, vision-language model (VLM)-driven exploration value estimation, high-level adaptive waypoint selection, and low-level action execution. Experiments on the HM3D benchmark and real-world environments demonstrate that RANGER achieves competitive performance in terms of navigation success rate and exploration efficiency, while showing superior ICL adaptability, with no previous 3D mapping of the environment required.

I. INTRODUCTION

Efficient visual target localization in complex environments is a core capability of embodied agents, with broad applications in service robotics, human–robot interaction, and autonomous monitoring systems. With the recent development of multimodal foundation models, including large language models (LLMs) (*e.g.,* [1], [2], [3], [4], [5]) and open-vocabulary vision models (*e.g.,* [6], [7], [8]), the performance of zero-shot object navigation (*e.g.,* [9], [10], [11], [12], [13], [14]) has significantly improved. Such methods allow robots to localize arbitrary objects without task-specific fine-tuning, thereby demonstrating strong potential for deployment in dynamic and previously unseen environments.

However, existing approaches still face major limitations. First, most methods rely heavily on depth sensing and precise pose estimation, usually involving global mapping/reconstruction, which are typically feasible only in simulation or with specialized hardware. In real-world scenarios, sensor noise, calibration errors, data collection,
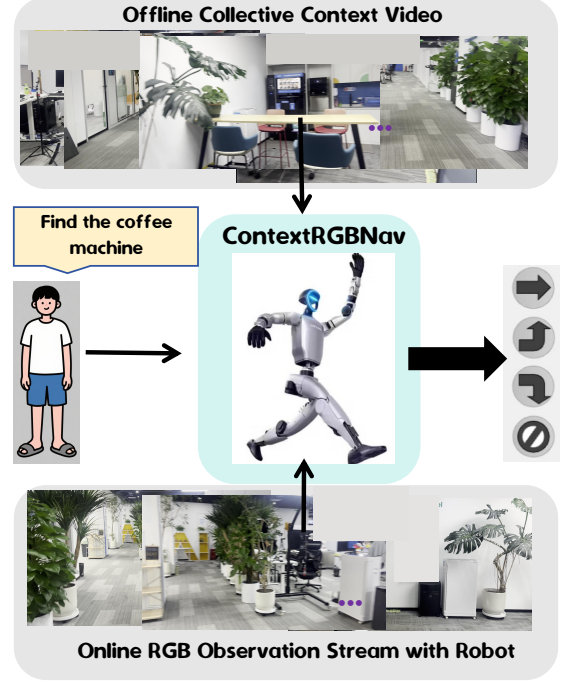
† Corresponding authors.

Fig. 1. RANGER Workflow: Given an offline video of a new environment captured with a camera (optionally) and an online RGB observation stream from the robot, RANGER efficiently adapts to the new environment and completes navigation tasks based on human instructions.

and hardware costs substantially restrict their practicality, similarly to indoor localization scenarios [15]. Second, current systems have yet to better leverage contextual knowledge available in everyday video streams, which can provide valuable priors for efficient exploration and rapid adaptation to novel environments.

This naturally raises a fundamental question: *Can a navigation framework be built relying solely on RGB input?* Such a framework would be inherently low-cost, easy to deploy, and capable of directly utilizing videos captured from arbitrary devices for rapid adaptation to new environments. Notably, recent data-driven methods such as MASt3R [16], Dust3R [17], Fast3R [18], and VGGT [19] have demonstrated remarkable performance and generalization in 3D reconstruction tasks, opening new opportunities to achieve efficient navigation with RGB-only input.

In this paper, we introduce **RANGER**: a zero-shot, open-

vocabulary semantic navigation framework based on monocular RGB input. Our approach requires neither depth sensors nor precise robot pose estimation, yet enables semantic-driven exploration and navigation in unseen environments. Furthermore, RANGER can adapt to a new environment using only a short offline video, significantly reducing exploration costs and enhancing navigation efficiency. Importantly, our method does not require any task-specific fine-tuning during navigation (see Fig. 1). Specifically, RANGER is built upon four key components: (1) online 3D reconstruction and localization from RGB-only input, (2) cross-frame semantic point cloud fusion, (3) high-level waypoint selection guided by vision–language models (VLMs), and (4) low-level action execution. At its core lies a *keyframe-based memory bank*, which encodes geometric, semantic, and exploration-value information of the environment. This memory is continuously curated and optimized in the backend to reduce errors and improve system robustness.

We conduct systematic evaluations on the large-scale HM3D dataset, demonstrating that RANGER achieves competitive performance without access to depth sensing, precise poses, nor global maps. In addition, we validate the practicality and robustness of our system in real-world environments such as meeting rooms and offices with a humanoid robot deployment. Our contributions are as follows:

- We propose RANGER, a zero-shot open-vocabulary semantic navigation framework that relies solely on monocular RGB input. Without requiring depth or pose information, it can navigate in unseen environments and rapidly adapt to new ones through short offline videos.
- We design a novel system architecture that integrates online RGB-based 3D reconstruction, semantic point cloud fusion, and VLM-guided hierarchical planning. Central to this architecture is a keyframe-based memory bank that jointly encodes geometry, semantics, and exploration value, and is continuously optimized for robust context-aware navigation.
- We conduct extensive experiments on the HM3D dataset and in real-world scenarios, demonstrating that RANGER achieves competitive navigation performance while exhibiting superior in-context learning capability compared to existing methods, utilizing only RGB data.

II. RELATED WORK

Object Goal Navigation. The task of locating a specified object in an unknown environment is widely applicable in robotic systems. Current approaches to object-goal navigation can be categorized into: (1) Approaches involving the use of pre-trained visual encoders to transform first-person observations into visual vectors, which are then processed by a navigation policy network through extensive imitation or supervised learning (*e.g.,* [20], [21], [22], [23], [24], [25], [26]), thereby equipping robots with semantic navigation abilities. However, these approaches suffer from overfitting to simulation environments, which limits their generalization to real-world settings. Additionally, they are constrained by predefined object categories, restricting their ability to

navigate to arbitrary unseen objects or visual targets. (2) Approaches that focus on Zero-Shot Object Navigation (*e.g.,* [9], [10], [13], [12], [14], [27], [28]). These methods explicitly construct environmental maps and utilize VLMs [2], [1], [3] or LLMs [4], [5] to select the most valuable frontier or waypoint for exploration. For instance, in Cow [10], the robot explores the nearest frontier point until the target is detected using CLIP features [29] and open-vocabulary object detectors [30]. ESC [31], L3MVN [11], and Voronav leverage LLMs for reasoning and decision-making to enhance performance. VLFM [13] employs a VLM to build semantic values on the map based on first-person observations and textual prompts, selecting the highest-scoring frontier. Their reliance on depth information, precise pose estimation, and task-specific fine-tuning often limits their performance in real-world scenarios, where depth data may be inaccurate or unavailable. These methods also hinder the ability to perform contextual learning, making it challenging for robots to leverage freely available monocular videos to improve exploration efficiency and adapt to new environments.

Monocular 3D Reconstruction. Monocular 3D reconstruction methods have made notable progress recently in enabling the building of 3D maps from single camera inputs. Techniques such as MASt3R [16], Dust3R [17], Fast3R [18], VGGT [19], MASt3R-SLAM [32], and VGGT-SLAM [33] have contributed significantly to this field. However, these methods often rely on passive reconstruction, where the trajectory is pre-collected and does not involve active perception or exploration. This restricts the system's ability to adapt to dynamic environments and limits its exploration capabilities. Unlike these systems, we aim to incorporate more active, adaptive learning to improve the navigation process without relying on pre-collected trajectories.

In-Context Learning. In-context learning (ICL), first demonstrated in large language models [34], allows models to perform tasks by leveraging a few examples provided in the input context, without requiring task-specific retraining. ICL has been successfully applied to a variety of tasks, including natural language understanding and object recognition. Recent work has extended this idea to robotics, where robots are trained to perform navigation tasks based on contextual information, such as video or textual prompts. For example, several works have used context from videos or previous maps to train navigation models [35]. However, these methods often require the target object to appear in the context, which severely limits their practical application, especially in situations where the object is not visible in the initial context. In contrast, our approach does not require the target object to appear, even in the collected offline video. Instead, it enables robots to decide whether to continue exploring or exploit the knowledge contained in the offline video to complete the navigation task. This adaptive approach makes RANGER more versatile, allowing it to handle a broader range of navigation scenarios without the need for predefined object categories or fine-tuning.

Fig. 2. Overview of RANGER: a unified architecture for zero-shot RGB-only navigation that builds geometric and semantic memory via a keyframe-based memory bank, which subsequently guides the agent's exploration.

III. PROBLEM FORMULATION

We consider two navigation tasks under a **zero-shot** setting, where agents are required to generalize without task-specific training. Both tasks involve navigating in previously unseen environments to locate a target, but differ in the availability of contextual information: the first relies solely on online RGB observations, while the second leverages an additional offline traversal video as prior context.

RGB Navigation. In the standard ObjectNav task with **RGB-only inputs**, an agent must navigate in an unseen environment to locate an object specified by a human-provided instruction. We denote the set of object categories as $C = \{c_0, \ldots, c_m\}$ and the set of scenes as $S = \{s_0, \ldots, s_m\}$. Each episode is defined as $T_i = \{s_i, c_i, p_i\}$, where the agent starts from a random position p_i in scene s_i with target category c_i. The agent receives only an RGB observation and the target category, without access to depth or pose information. The action space A includes six discrete actions: *move forward*, *turn left*, *turn right*, *look up*, *look down*, and *stop*. The *move forward* action moves the agent by 25 cm, while *turn* actions adjust orientation by 30°. An episode is considered successful if the agent issues a *stop* action when the geodesic distance to the target is below a predefined threshold, with a trajectory length within the steps limit.

Contextual RGB Navigation. In the contextual variant, the agent is additionally provided with an offline traversal video V_s of a human exploring a novel environment s. The task then requires locating the target object by combining prior visual context from the offline video with real-time RGB observations. This formulation enables the agent to reduce redundant exploration and achieve more efficient navigation and object localization in unseen environments.

IV. METHODOLOGY

A. Overview of the Process

RANGER employs a unified architecture that seamlessly handles both *zero-shot RGB-only navigation* and *video-context-augmented navigation* without requiring any architectural modifications or retraining. The system maintains a dynamic keyframe bank, which serves as a joint geometric and semantic memory of the environment. Upon receiving each new RGB observation, the backend refines the agent's pose in real-time and performs loop closure by optimizing relative poses against the stored keyframes. This process incrementally constructs a dense 3D map, enabling metric self-localization. Simultaneously, a semantic module aggregates object features via CLIP [29] and GroundingDINO [6] into a semantic point cloud, where each point is annotated with category likelihoods and spatial context, creating a queryable semantic memory. To facilitate efficient path planning, a 2D occupancy map is projected from the 3D reconstruction. The hierarchical planner selects high-level waypoints by considering the human-provided goal description, semantic similarity scores of observed regions, and spatial confidence regarding object presence, while a low-level controller translates each waypoint into discrete atomic actions. This perception-planning-action loop operates continuously in real-time until

the agent executes the *stop* action, marking the achievement of high-confidence visual goal localization.

B. Online RGB Reconstruction and Localization

To enable metric-aware navigation from monocular RGB inputs, we integrate **MASt3R-SLAM** [32], a state-of-the-art real-time dense SLAM system based on the MASt3R two-view 3D reconstruction prior. Its open-source implementation is directly incorporated into RANGER as a plug-and-play geometric backbone.

Keyframe-Based Reconstruction. MASt3R-SLAM selects dynamic keyframes based on visual novelty and tracking confidence. For each incoming RGB frame, it predicts dense pointmaps via the MASt3R network and matches them against the current keyframe using an efficient iterative projective matching scheme. This enables real-time 3D scene reconstruction without depth sensors or camera calibration.

Localization. The agent's 6-DoF pose is continuously estimated by minimizing ray-based reprojection errors between predicted pointmaps and the canonical keyframe geometry. This method is robust to depth prediction noise and operates under a generic central camera model, making it ideal for uncalibrated real-world deployment.

Global Consistency via Backend Optimization To mitigate drift and ensure long-term consistency, MASt3R-SLAM ensures long-term consistency through second-order global optimization over a pose graph, constructed from sequential and loop-closure edges. Loop candidates are retrieved using ASMK [36] on dense visual features and validated via geometric matching.

Real-Scale Reconstruction. Since monocular reconstruction lacks real scale, we utilize the robot's camera height as prior knowledge to compute the real scale of the 3D map. We select the lowest 20% of points based on their y-coordinates as candidate ground points. Using the RANSAC algorithm, we fit a plane to these points and estimate the plane coefficients a, b, c, and d. We then compute the ground height h_{ground} as:

$$h_{\text{ground}} = \frac{|d|}{\sqrt{a^2 + b^2 + c^2}}.$$

Using the real camera height h_{real}, the point cloud's real scale is calculated as $\frac{h_{\text{real}}}{h_{\text{ground}}}$.

C. Object Point Cloud Merge

We first employ Grounding DINO as an open-vocabulary detector and combine it with Mobile SAM [7] to extract object masks within the detection boxes of each keyframe stored in the memory bank. Then, using the keyframe confidence masks provided by MASt3R-SLAM, we filter these object regions to obtain high-confidence object point cloud representations in 3D space. For each semantic mask, we further crop the corresponding image region and extract visual features with CLIP. This process ultimately generates a semantic point cloud along with class confidence scores and target category information.

Object Association. For each newly detected object j, we compute both geometric and semantic similarity to existing objects. Geometric similarity S_{geo} is based on the Intersection over Union (IoU) of the point clouds, while visual similarity S_{vis} is determined by comparing the semantic features of the newly detected object with those of existing objects. The overall similarity score is a weighted sum:

$$s(i, j) = w_1 S_{\text{vis}}(i, j) + w_2 S_{\text{geo}}(i, j),$$

where w_1 and w_2 are weights. If the similarity score falls below a predefined threshold τ, a new object is initialized. Otherwise, the new detection is associated with the existing object exhibiting the highest similarity.

Object Fusion. For associated objects, their point clouds are merged, and their features are updated via a weighted average based on detection frequency.

D. 2D Map Generation

Frontier Map. After constructing a unified 3D point cloud, we project the points onto a 2D plane to create obstacle and exploration maps. Points above the floor are projected onto the obstacle map, while all points contribute to the exploration map. Frontiers are generated by detecting the boundaries between explored and unexplored regions. As the robot explores, the locations of frontiers dynamically change until the environment is fully explored.

Value Map. For each keyframe in the memory bank, we compute a matching score to the target instruction to measure the relevance between the corresponding region and the target category. The high-confidence point cloud associated with each keyframe is then reconstructed in 3D space and projected back into 2D, producing a 2D value map that guides agents' exploration.

E. High-Level Planner for Adaptive Waypoint Selection

To enable robust navigation under perceptual uncertainty, we design a high-level planner that dynamically selects waypoints by integrating *semantic relevance*, *geometric accessibility*, and *failure-aware blacklist management*. The planner operates on the dense 2D map and agent pose provided by MASt3R-SLAM. At each planning step t, the planner considers a set of candidate waypoints $\mathcal{W}_t = \mathcal{O}_t \cup \mathcal{F}_t$, where $\mathcal{O}_t$ represents object proposals and $\mathcal{F}_t$ denotes frontier points. It also takes as input the agent's current pose T_t from MASt3R-SLAM, together with a dynamic blacklist $\mathcal{B}_t$ that records previously unreachable waypoints. The final waypoint is determined by combining the value map with the semantic confidence of objects, which jointly evaluate and rank the candidates to select the most promising one.

F. Path Planning

We use the Fast Marching Method (FMM) [37] as the local planner to generate a path toward the goal. At each step, the robot executes motion commands toward a local subgoal, while the map and target are updated in real time—enabling adaptive, closed-loop navigation in partially observed environments.

(a) 3D Map at step 127 **(b) Frontier Map at step 127** **(c) Value Map at step 127** **(d) The first view image at step 127**
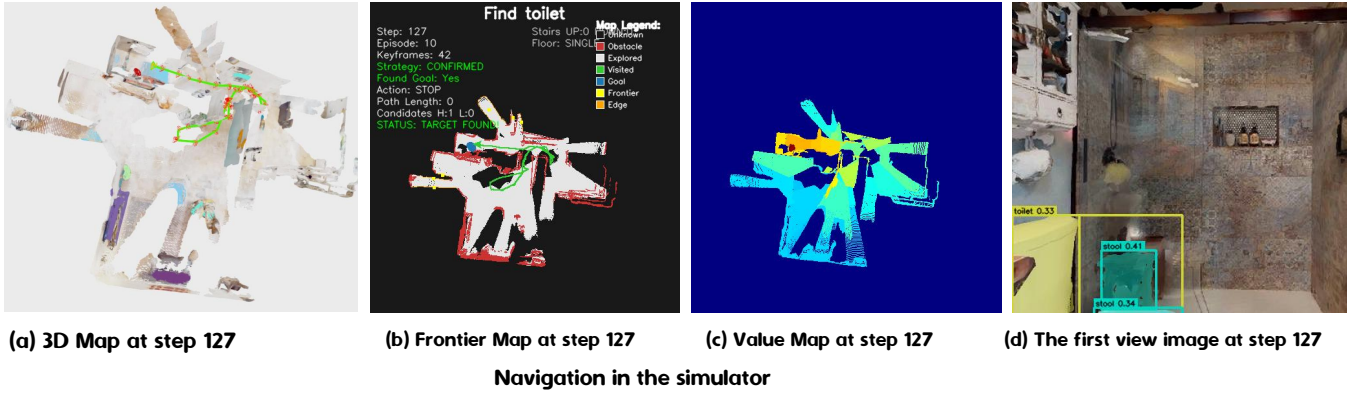
Navigation in the simulator

Fig. 3. Visualization of the navigation process in a simulated environment with task instruction: "Find the toilet". (a) Reconstructed 3D map and the agent's trajectory at step 127. The red cones represent keyframe locations, while the green cone indicates the agent's current position. The green line traces the agent's movement, and the red point cloud represents the toilet object. (b) The Frontier Map showing the robot's exploration trajectory. The blue area highlights the target object region, red areas indicate obstacles, and yellow dots represent frontier points. (c) The Value Map, where red regions correspond to high-value areas. (d) First-person observation.

V. EXPERIMENTS

We evaluate RANGER on object goal navigation tasks across both simulated and real-world environments, testing its navigation performance in completely unseen settings, as well as when provided with a contextual video.

A. Simulation-based Experiment Setup

Navigation in unseen environments. We evaluate our approach on the Habitat HM3Dv2 dataset (HM3D-Semantics-v0.2 [38], released in the 2023 Habitat Challenge), which includes six goal categories. For our experiments, we select 10 single-floor scenes comprising 279 episodes in total. In each episode, the agent's starting position is randomly sampled to assess navigation performance in previously unseen environments. Considering the trade-off between system storage and performance, we set the maximum episode length to 300 steps.

Navigation with contextual video. We use the same 10 scenes and manually collect one video trajectory per scene by teleoperating the robot in the simulator. For evaluation, the agent is initialized near the endpoint of the collected video to ensure partial overlap between the agent's initial observation and the video frames, which facilitates re-localization. For each scene, we randomly sample 2 or 3 starting positions near the video endpoint, resulting in 100 episodes in total across 6 object categories.

B. Metrics

We use navigation success rate (SR) and success rate weighted by navigation path length (SPL) as evaluation metrics. SR represents the percentage of successful episodes out of the total episodes. SPL measures the efficiency of reaching the goal in addition to the success rate.

C. Implementation Details

In the Habitat simulation environment, the agent perceives the scene through an RGB camera with a resolution of 640×480 pixels, mounted at a height of 0.88 above the ground plane. For semantic segmentation, we leverage Grounding DINO [6] to generate class-agnostic object proposals and MobileSAM [7] to produce pixel-accurate masks. Semantic confidence scores for detected objects are computed using CLIP [29], enabling zero-shot semantic grounding. Our system employs consistent hyper-parameters: keyframe selection threshold $\omega_k = 0.333$, loop-closure detection threshold $\omega_l = 0.1$, and robustness regularization weight $\omega_r = 0.005$. To ensure reliable relocalization, we enforce a stricter geometric consistency check when attaching the current frame to the pose graph: the ratio of inlier feature matches must exceed 0.3. In addition, the confidence threshold for the point cloud is set to 1.9.

VI. RESULTS
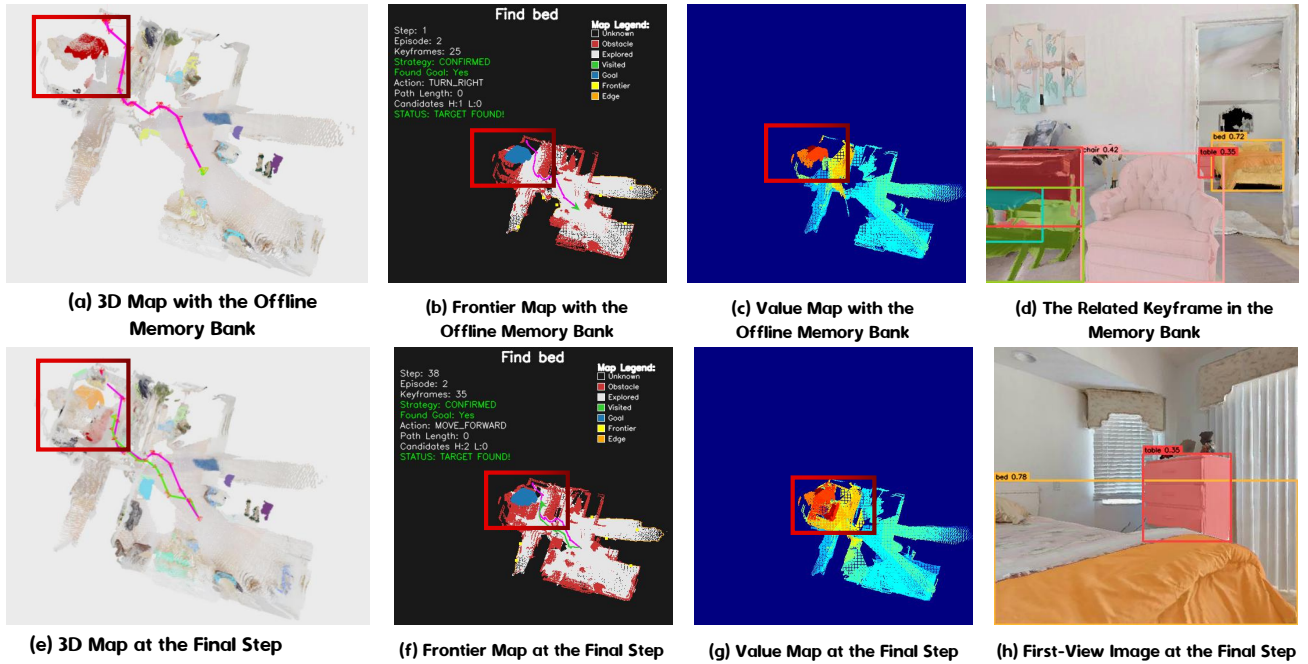
A. Navigation in Unseen Environments

Previously, zero-shot object navigation heavily relied on accurate pose and depth information provided by simulators. To evaluate our approach in more realistic settings, we compare with L3MVN [11], a representative work that utilizes LLMs for efficient frontier selection and requires privileged inputs (depth and pose). As detailed in Table I, L3MVN (300) and L3MVN (500) represent performance under step limits of 300 and 500, respectively, both leveraging RGB, depth, and pose data. In contrast, RANGER operates solely on RGB input, without any privileged sensing.

TABLE I
PERFORMANCE METRICS OF NAVIGATION IN UNSEEN ENVIRONMENTS.

Methods	Sensors	SR	SPL	Avg Steps
L3MVN (300)	RGB, Depth, Pose	39.4	15.7	147.62
L3MVN (500)	RGB, Depth, Pose	42.3	16.3	171.06
RANGER (300)	RGB	42.7	17.8	172.80

As presented in Table I, RANGER achieves an SR of 42.7% and an SPL of 17.8% under the 300-step limit. This performance significantly outperforms L3MVN (300) by 3.3

(a) 3D Map with the Offline Memory Bank

(b) Frontier Map with the Offline Memory Bank

(c) Value Map with the Offline Memory Bank

(d) The Related Keyframe in the Memory Bank

(e) 3D Map at the Final Step

(f) Frontier Map at the Final Step

(g) Value Map at the Final Step

(h) First-View Image at the Final Step

Adapting navigation to new environments using only an offline video.

Fig. 4. Contextual adaptation for zero-shot navigation in a new environment. RANGER can leverage an offline video to adapt and locate the target object "bed". (a-d) Initial state with offline memory; (e-h) Final navigation state. The system successfully found the target in 38 steps.

percentage points in SR. Notably, RANGER even surpasses L3MVN (500), which benefits from both an extended step limit and privileged sensor inputs. These compelling results underscore that integrating contextual video priors enables competitive navigation performance in previously unseen environments using only standard RGB input. Figure 3 visually depicts a navigation instance: the agent successfully reaches the *toilet* at step 127, with 42 frames stored in its keyframe-based memory bank. The highlighted region in Figure 3 (c) further confirms the strong spatial consistency between the agent's memory and the observed environment, illustrating effective visual grounding.

B. Navigation with a Contextual Video

TABLE II
PERFORMANCE COMPARISON WITH AND WITHOUT CONTEXTUAL VIDEO.

Methods	SR	SPL	DTG	Avg Steps
w/o video	44.0	16.4	2.933	171.36
w/ video	58.0	30.2	2.381	110.22

Table II presents the navigation performance with and without contextual video. When no video is provided, the agent achieves a success rate (SR) of 44.0 and requires on average 171.4 steps. By contrast, incorporating an offline traversal video significantly improves performance, yielding an SR of 58.0, a higher SPL of 30.2, and a shorter average trajectory of 110.2 steps. These results confirm that contextual videos effectively reduces redundant exploration and guides the agent toward more efficient navigation. In our

framework, offline videos serve as an *environmental preview*. By constructing a keyframe-based memory bank, the system acquires prior knowledge of the scene before navigation, thereby reducing redundant exploration. This mechanism mimics the way humans navigate more efficiently in a new environment after watching a walkthrough video. In practice, we observe that providing such contextual information enables the agent to significantly reduce unnecessary exploration and complete target-finding tasks more efficiently. As illustrated in Fig. 4, when searching for a *bed*, RANGER first builds a keyframe memory bank from the offline video and applies semantic retrieval to identify the target object within the video. The object is then transformed into a point cloud representation, which is integrated with both the offline video and real-time observations to construct an environment map. Finally, the system plans a collision-free path that directly leads the agent to the target location.

C. Ablation Studies

Reconstruction and Localization Accuracy As shown in Fig. 5, we compare the latest 3D reconstruction methods—VGGT, VGGT-SLAM, and MASt3R-SLAM—with the Ground Truth (GT). The video trajectories are collected by a manually teleoperated agent navigating within the environment. The results demonstrate that VGGT suffers from insufficient detail modeling and, due to its requirement to process the entire video sequence at once, fails to meet the real-time demands of navigation tasks. In contrast, VGGT-SLAM constructs dense 3D maps and performs localization by incrementally aligning submaps generated by VGGT. However, in long-sequence scenarios, the submap merging process often introduces significant alignment errors, limiting

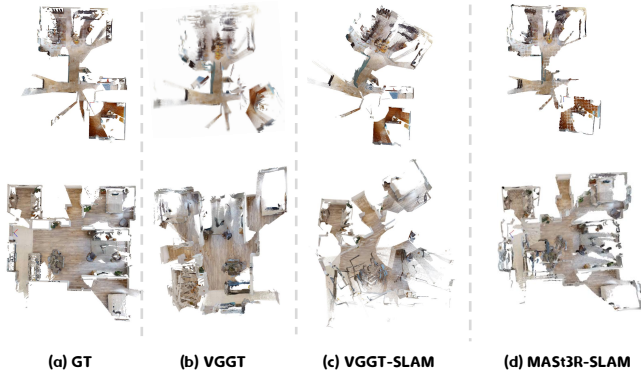**(a) GT**   **(b) VGGT**   **(c) VGGT-SLAM**   **(d) MASt3R-SLAM**

Fig. 5. Comparison of 3D maps reconstructed using different methods. Figure (a) shows the result using real depth and pose data. Figures (b), (c), and (d) present the reconstruction results of VGGT, VGGT-SLAM, and MASt3R-SLAM, respectively, all relying solely on RGB images.

its effectiveness. MASt3R-SLAM exhibits stronger robustness under the same conditions. It consistently achieves higher reconstruction quality and global consistency across trajectories of varying lengths, effectively mitigating drift and distortion issues commonly observed in long-sequence stitching. Moreover, it supports real-time operation, making it suitable for navigation applications.

Component Analysis. Table III summarizes the ablation results for two key components: the high-level planner and the object detector. When the high-level planner is removed, performance drops considerably (SR = 34.7%, SPL = 15.3%), and the average steps increase from 172.80 to 202.83. This confirms the critical role of the planner in efficiently guiding the agent toward the target. For the detector comparison, YOLO-World [8] and DINO yield relatively close results, with DINO showing a slight advantage (SR = 42.7%, SPL = 17.8% vs. 41.7%, 16.7%). This suggests that while replacing the detector has only a modest impact on overall accuracy, stronger visual grounding from DINO provides more consistent navigation performance.

TABLE III
IMPACT OF MODEL COMPONENTS.

component	SR	SPL	DTG	Avg Steps
w/o High Level Planner	39.8	18.6	3.552	184.43
YOLO-World	42.3	17.1	3.573	178.06
DINO	42.7	17.8	3.366	172.80

Effect of Step Limits. As the step limit increases, the memory bank must maintain a growing number of keyframe point clouds, poses, semantic segmentation, and their associated values, potentially leading to substantial storage and computation overhead. Based on this consideration, we evaluate RANGER under different maximum step limits. As shown in Table IV, the success rate (SR) improves steadily with larger step budgets, rising from 6.1% at 50 steps to 42.7% at 300 steps. This indicates that a longer execution horizon provides the agent with more opportunities for exploration. However, the improvement becomes marginal

beyond 250 steps; therefore, we set the maximum step limit to 300 in our experiments.

TABLE IV
SR UNDER DIFFERENT MAXIMUM STEP LIMITS.

Max Steps	50	100	200	250	300
SR	0.061	0.222	0.366	0.401	0.427

D. Navigation in the Real World

Real-World Experiment Setup. We validate the practicality of RANGER through real-world experiments on a Unitree G1 humanoid robot, equipped with an Intel RealSense D455 RGB-D camera mounted at a height of 1.29 m on a custom 2 DoF head. Importantly, *only the RGB stream is used* for sensing and navigation, consistent with our depth-free assumption. All system components—including MASt3R-SLAM for online 3D reconstruction, CLIP, and Grounding DINO for semantic grounding, and MobileSAM for instance-aware segmentation—are deployed on a mobile workstation with an NVIDIA RTX 4090 Laptop GPU and an Intel Core i9-13900HX CPU, achieving real-time inference at approximately 1 Hz. The experiments were carried out in diverse indoor environments, including laboratories and meeting rooms, where the robot was instructed to navigate toward semantically defined targets (*e.g.,* "find a chair," "find the potted plant").

Visualization. Representative qualitative results are shown in Fig. 6. In the example task, the user instructs the robot to locate a *plant*. After completing exploration of the first room (step 51), the robot autonomously selects a high-value frontier region and transitions to an adjacent room, successfully detecting the target at step 76. Notably, the high-value region highlighted in Fig. 6 (c) aligns closely with the actual target location shown in Fig. 6 (b), demonstrating the effectiveness of semantic information in guiding exploration.

VII. CONCLUSIONS AND LIMITATIONS

In this work, we introduce RANGER, a novel zero-shot visual target navigation framework relying solely on RGB input. RANGER significantly enhances navigation efficiency without task-specific fine-tuning through its keyframe-based memory bank, back-end optimization, keyframe-driven reconstruction, and hierarchical planning strategy. The system also demonstrates rapid adaptation and substantial performance gains with only a short video sequence of a new environment, offering a new perspective on zero-shot navigation. Ultimately, this work presents a practical pathway toward real-world autonomous navigation and opens new directions for research focused purely on visual input.

Limitations. Despite the strong performance and contextual learning capability of RANGER, several limitations remain. First, the continuous accumulation of keyframes increases storage overhead and may degrade system efficiency over time, highlighting the need for more effective memory management strategies. Second, reconstruction and
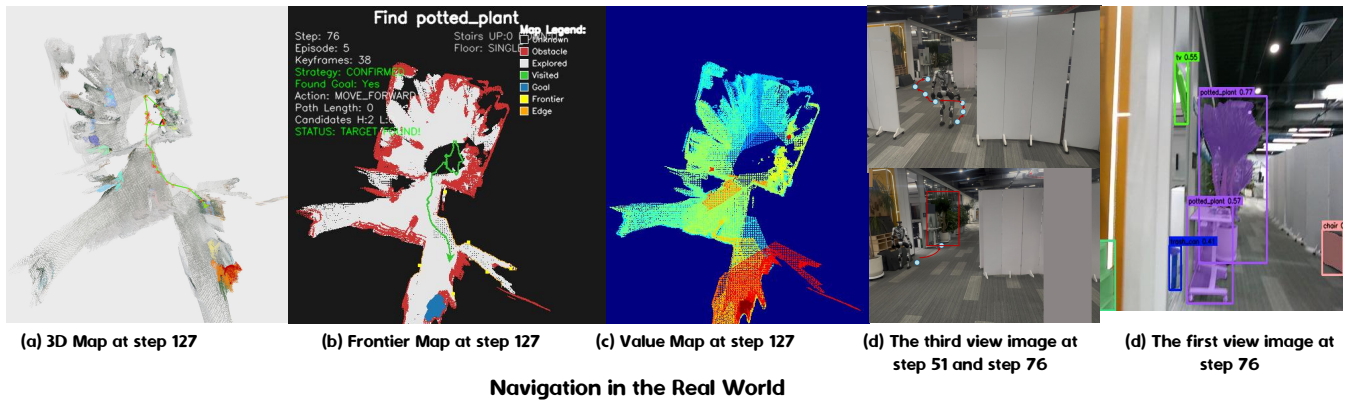
(a) 3D Map at step 127   **(b) Frontier Map at step 127**   **(c) Value Map at step 127**   **(d) The third view image at step 51 and step 76**   **(d) The first view image at step 76**

Navigation in the Real World

Fig. 6. Real-world navigation with RANGER on a Unitree G1 humanoid robot. Task: "Find potted plant.".

localization remain possible bottlenecks for purely RGB-based navigation, as their robustness is still insufficient to handle overly complex or dynamic environments. Enhancing the reliability of these modules will be critical for advancing the practical deployment of such systems.

REFERENCES

[1] OpenAI, "Gpt-4 technical report," *arXiv preprint arXiv:2303.08774*, 2023.

[2] H. Liu, C. Li, Q. Wu, and Y. J. Lee, "Visual instruction tuning," *NeurIPS*, vol. 36, pp. 1–19, 2023.

[3] J. Bai, S. Bai, S. Yang, S. Wang, S. Tan, P. Wang, J. Lin, C. Zhou, and J. Zhou, "Qwen-vl: A frontier large vision-language model with versatile abilities," *arXiv preprint arXiv:2308.12966*, 2023.

[4] A. Dubey, A. Jauhri, A. Pandey, A. Kadian, A. Al-Dahle, A. Letman, A. Mathur, A. Schelten, A. Yang, A. Fan *et al.*, "The llama 3 herd of models," *arXiv preprint arXiv:2407.21783*, 2024.

[5] G. Team, R. Anil, S. Borgeaud, J.-B. Alayrac, J. Yu, R. Soricut, J. Schalkwyk, A. M. Dai, A. Hauth, K. Millican *et al.*, "Gemini: a family of highly capable multimodal models," *arXiv preprint arXiv:2312.11805*, 2023.

[6] S. Liu, Z. Zeng, T. Ren, F. Li, H. Zhang, J. Yang, Q. Jiang, C. Li, J. Yang, H. Su *et al.*, "Grounding dino: Marrying dino with grounded pre-training for open-set object detection," in *ECCV*, 2024, pp. 38–55.

[7] A. Kirillov, E. Mintun, N. Ravi, H. Mao, C. Rolland, L. Gustafson, T. Xiao, S. Whitehead, A. C. Berg, W.-Y. Lo *et al.*, "Segment anything," in *ICCV*, 2023, pp. 4015–4026.

[8] T. Cheng, L. Song, Y. Ge, W. Liu, X. Wang, and Y. Shan, "Yoloworld: Real-time open-vocabulary object detection," in *CVPR*, 2024, pp. 16901–16911.

[9] Y. Kuang, H. Lin, and M. Jiang, "Openfmnav: Towards open-set zero-shot object navigation via vision-language foundation models," *arXiv preprint arXiv:2402.10670*, 2024.

[10] S. Y. Gadre, M. Wortsman, G. Ilharco, L. Schmidt, and S. Song, "Cows on pasture: Baselines and benchmarks for language-driven zero-shot object navigation," in *CVPR*, vol. 2023-June, 2023, pp. 23171–23181.

[11] B. Yu, H. Kasaei, and M. Cao, "L3mvn: Leveraging large language models for visual target navigation," in *IROS*, 2023, pp. 3554–3560.

[12] P. Wu, Y. Mu, B. Wu, Y. Hou, J. Ma, S. Zhang, and C. Liu, "Voronav: Voronoi-based zeroshot object navigation with large language model," in *ICML*, 2024.

[13] N. Yokoyama, S. Ha, D. Batra, J. Wang, and B. Bucher, "Vlfm: Vision-language frontier maps for zero-shot semantic navigation," in *ICRA*, 2024, pp. 42–48.

[14] H. Yin, X. Xu, L. Zhao, Z. Wang, J. Zhou, and J. Lu, "Unigoal: Towards universal zero-shot goal-oriented navigation," *CVPR*, 2025.

[15] Y. Shu, Z. Li, B. F. Karlsson, Y. Lin, T. Moscibroda, and K. Shin, "Incrementally-deployable indoor navigation with automatic trace generation," in *IEEE INFOCOM*, 2019, pp. 2395–2403.

[16] V. Leroy, Y. Cabon, and J. Revaud, "Grounding image matching in 3d with mast3r," in *ECCV*, 2024, pp. 71–91.

[17] S. Wang, V. Leroy, Y. Cabon, B. Chidlovskii, and J. Revaud, "Dust3r: Geometric 3d vision made easy," in *CVPR*, 2024, pp. 20697–20709.

[18] J. Yang, A. Sax, K. J. Liang, M. Henaff, H. Tang, A. Cao, J. Chai, F. Meier, and M. Feiszli, "Fast3r: Towards 3d reconstruction of 1000+ images in one forward pass," in *CVPR*, 2025, pp. 21924–21935.

[19] J. Wang, M. Chen, N. Karaev, A. Vedaldi, C. Rupprecht, and D. Novotny, "VGGT: Visual geometry grounded transformer," in *CVPR*, 2025, pp. 5294–5306.

[20] K. Yadav, A. Majumdar, R. Ramrakhya *et al.*, "Ovrl-v2: A simple state-of-the-art baseline for imagenav and objectnav," *arXiv preprint arXiv:2303.07798*, 2023, version 2.

[21] R. Ramrakhya, D. Batra, E. Wijmans *et al.*, "Pirlnav: Pretraining with imitation and rl finetuning for objectnav," in *CVPR*, 2023, pp. 17896–17906.

[22] J. Zhang, K. Wang, R. Xu, G. Zhou, Y. Hong, X. Fang, Q. Wu, Z. Zhang, and H. Wang, "Navid: Video-based vlm plans the next step for vision-and-language navigation," *RSS*, 2024.

[23] D. Batra, A. Gokaslan, A. Kembhavi, O. Maksymets, R. Mottaghi, M. Savva, A. Toshev, and E. Wijmans, "Objectnav revisited: On evaluation of embodied agents navigating to objects," *arXiv preprint arXiv:2006.13171*, 2020.

[24] K. Ehsani, T. Gupta, R. Hendrix *et al.*, "Spoc: Imitating shortest paths in simulation enables effective navigation and manipulation in the real world," *arXiv preprint arXiv:2312.02976*, 2023.

[25] S. Chen, T. Chabal, I. Laptev *et al.*, "Object goal navigation with recursive implicit maps," in *IROS*, 2023, pp. 7089–7096.

[26] J. Huang, S. Yong, X. Ma, X. Linghu, P. Li, Y. Wang, Q. Li, S.-C. Zhu, B. Jia, and S. Huang, "An embodied generalist agent in 3d world," *arXiv preprint arXiv:2311.12871*, 2023.

[27] H. Yuan, Y. Bai, Y. Fu, B. Zhou, Y. Feng, X. Xu, Y. Zhan, B. F. Karlsson, and Z. Lu, "Being-0: A humanoid robotic agent with vision-language models and modular skills," *arXiv preprint arxiv:2503.12533*, 2025. [Online]. Available: https://arxiv.org/abs/2503.12533

[28] K.-H. Zeng, Z. Zhang, K. Ehsani, R. Hendrix, J. Salvador, A. Herrasti, R. Girshick, A. Kembhavi, and L. Weihs, "Poliformer: Scaling on-policy rl with transformers results in masterful navigators," *CoRL*, 2024.

[29] A. Radford, J. W. Kim, C. Hallacy, A. Ramesh, G. Goh, S. Agarwal, G. Sastry, A. Askell, P. Mishkin, J. Clark *et al.*, "Learning transferable visual models from natural language supervision," in *International conference on machine learning*. PmLR, 2021, pp. 8748–8763.

[30] M. Caron, H. Touvron, I. Misra, H. Jégou, J. Mairal, P. Bojanowski, and A. Joulin, "Emerging properties in self-supervised vision transformers," in *ICCV*, 2021.

[31] K. Zhou, K. Zheng, C. Pryor, Y. Shen, H. Jin, L. Getoor, and X. E. Wang, "Esc: Exploration with soft commonsense constraints for zero-shot object navigation," in *ICML*, 2023, pp. 42829–42842.

[32] R. Murai, E. Dexheimer, and A. J. Davison, "MASt3R-SLAM: Real-time dense SLAM with 3D reconstruction priors," in *CVPR*, 2025, pp. 16695–16705.

[33] D. Maggio, H. Lim, and L. Carlone, "VGGT-SLAM: Dense RGB SLAM optimized on the SL(4) manifold," *arXiv preprint arXiv:2505.12549*, 2025.

[34] T. Brown, B. Mann, N. Ryder, M. Subbiah, J. D. Kaplan, P. Dhariwal, A. Neelakantan, P. Shyam, G. Sastry, A. Askell *et al.*, "Language models are few-shot learners," *Advances in Neural Information Processing Systems*, vol. 33, pp. 1877–1901, 2020.

[35] B. Zhou, Z. Zhang, J. Wang, and Z. Lu, "Nolo: Navigate only look once," *arXiv preprint arXiv:2408.01384*, 2024.

[36] G. Tolias, Y. Avrithis, and H. Jégou, "To aggregate or not to aggregate: Selective match kernels for image search," in *Proceedings of the IEEE international conference on computer vision*, 2013, pp. 1401–1408.

[37] J. A. Sethian, "A fast marching level set method for monotonically advancing fronts." *Proceedings of the National Academy of Sciences*, vol. 93, no. 4, pp. 1591–1595, 1996.

[38] K. Yadav, R. Ramrakhya, S. K. Ramakrishnan, D. Batra, Y. Bisk, and R. Mottaghi, "Habitat-matterport 3d semantics dataset," in *CVPR*, 2023, pp. 4927–4936.